AWARD NUMBER:  W81XWH-12-C-0043


TITLE: Ultraviolet Communication for Medical Applications



PRINCIPAL INVESTIGATOR   Jeff Guy
                                             Directed Energy, Inc.


CONTRACTING ORGANIZATION:  USAMRMC


REPORT DATE:  June 2015


TYPE OF REPORT:  Final, Phase II


PREPARED FOR:  U.S. Army Medical Research and Materiel Command
                             Fort Detrick, Maryland  21702-5012


DISTRIBUTION STATEMENT A: Approved for Public Release;
                                               Distribution Unlimited

# REPORT DOCUMENTATION PAGE

*Form Approved*
*OMB No. 0704-0188*

| 1. REPORT DATE | 2. REPORT TYPE | 3. DATES COVERED *(From - To)* |
|---|---|---|
| June 2015 | Final | MAY 1, 2013 to APR 30, 2015 |

| 4. TITLE AND SUBTITLE | |
|---|---|
| Ultraviolet Communication for Medical Applications | **5a. CONTRACT NUMBER** W81XWH-12-C-0043 |
| | **5b. GRANT NUMBER** |
| | **5c. PROGRAM ELEMENT NUMBER** |

| 6. AUTHOR(S) | |
|---|---|
| Jeff Guy | **5d. PROJECT NUMBER** |
| Carol Wedding | **5e. TASK NUMBER** |
| | **5f. WORK UNIT NUMBER** |

| 7. PERFORMING ORGANIZATION NAME(S) AND ADDRESS(ES) | 8. PERFORMING ORGANIZATION REPORT NUMBER |
|---|---|
| Directed Energy, Inc. (DEI) 1500 Bull Lea Rd STE 212 Lexington, KY 40511-1267 | |

| 9. SPONSORING / MONITORING AGENCY NAME(S) AND ADDRESS(ES) | 10. SPONSOR/MONITOR'S ACRONYM(S) |
|---|---|
| U.S. Army Medical Research and Materiel Command (USAMRMC) Fort Detrick, MD 21702-5012 | USAMRMC |
| | 11. SPONSOR/MONITOR'S REPORT NUMBER(S) |

**12. DISTRIBUTION / AVAILABILITY STATEMENT**
DISTRIBUTION A: Approved for Public Release; Distribution Unlimited

**13. SUPPLEMENTARY NOTES**
Report contains color.

**14. ABSTRACT**

Under this Phase II SBIR effort, Directed Energy Inc.'s (DEI) proprietary ultraviolet (UV) emitters and the best available electro-optic components are investigated to implement a functional prototype demonstrating short range, medium data rate non-line-of-sight (NLOS) optical communication data links operating in the solar blind region (200–280 nm). The intended application is covert wireless transfer of medical data for battlefield combat casualty care. During the course of this effort and after detailed investigation pertinent to this technology through simulation, system studies, field trials, and review of current and future technologies, hardware components were designed and integrated into a functional breadboard system demonstrating: (1) unidirectional communication of medical data in outdoors environment; and (2) bidirectional communication of medical data with encryption and forward error correction. Work in the second half of the Phase II project will extend the test bench implementation to be capable of mobile ad-hoc networking, and will repackage the system as a brassboard module suitable for field trials.

**15. SUBJECT TERMS**
Non-line-of-sight (NLOS), networking, optical communication, plasma-shells, short range, ultraviolet (UV) light

| 16. SECURITY CLASSIFICATION OF: | | | 17. LIMITATION OF ABSTRACT | 18. NUMBER OF PAGES | 19a. NAME OF RESPONSIBLE PERSON |
|---|---|---|---|---|---|
| **a. REPORT** Unclassified | **b. ABSTRACT** Unclassified | **c. THIS PAGE** Unclassified | UU | 16 | **19b. TELEPHONE NUMBER** *(include area code)* |

**Standard Form 298 (Rev. 8-98)**
Prescribed by ANSI Std. 239.18

## Table of Contents

# Introduction

This project investigates the efficacy of short range (up to 50 m), medium data rate (at least 57.6 kbps) non-line-of-sight (NLOS) optical data communication using ultraviolet (UV) light in the solar blind region (200–280 nm wavelength). The application is wireless transfer of medical data for battlefield combat casualty care. The investigated scenario is medical data transfer between a patient-worn vital sign monitor to a medic PDA from the initial site of trauma in outdoor environments with diverse atmospheric conditions to indoor areas including evacuation vehicles and forward combat support hospitals. With the exception of work conducted under this project, no researchers have experimentally demonstrated compact untethered transceivers capable of adequate range and data rate.

# Body

Under this Phase II SBIR, DEI's main objective was to develop prototype UV optical communication hardware to create a flexible hardware platform that can be easily integrated into a variety of applications relevant to the Army medical mission.

## Task 1. Simulation

Monte Carlo photon scattering simulation requires considerable processing power to accurately model high path loss. DEI employed a high-end simulation computer, CUDA processing library and wrote custom photon scatter code for parallel execution on a graphics processing unit (GPU).

The working Monte Carlo (MC) photon scatter code was validated against current published research. The working Monte Carlo (MC) photon scatter code was then ported to MATLAB to use the Parallel Processing Toolbox that allows code to run on multiple CPU and GPU cores.

 As a first step the C code was rewritten from a form based on sequential branching code, to a non-branching matrix form. This eliminates code branches that incur a significant performance penalty, and uses matrix operations that scale well on parallel hardware. Execution time was reduced from 450 minutes per billion photons with the C code running on 4 CPU cores, to 4.5 minutes per billion photons with the MATLAB code running on 192 GPU cores. Additional tweaks realized a speedup of

~30X; In the future, the code will be used to explore design tradeoffs as we work to miniaturize the system.

## Task 2. Plasma-shell Improvement

The primary areas investigated included electroding, investigation of phosphors, and driving the shells. DEI also conducted extended life testing of the shells.

### Electroding

It was demonstrated in the Phase I Option that our novel three-electrode Plasma-shell pattern shown in Figure 1 will provide the following benefits: higher UVC emission per component, higher drive efficiency, high-speed addressability of the entire Plasma-shell array, and scalable array power emission. This directly supports performance objectives of longer communication range and reduced power consumption.



Figure 1. Plasma-shell with three-electrode pattern.

The Phase II effort began with measuring the Plasma-shell process variation in order to specify tooling and shell handling equipment for the three-electrode system because the new pattern cannot be printed in the same way as the conventional two-electrode pattern. Nominal shell dimensions were 4.40 mm × 2.25 mm (W × H) with ± 0.04 mm tolerance as measured from hundreds of shells, and this is acceptable for automated printing and handling. Next, the option of having our shells electroded by an external company was investigated and DEI accordingly contracted Microtech, a specialist in handling and applying electrodes to surface-mount components, to investigate the feasibility of high-volume electroding (150,000 Plasma-shells per day). A trial run of 1800 non-lighting shells demonstrated very good electrode quality, and Microtech provided positive feedback about the manufacturability of the machine-printed electrode pattern.

### Drive System

Shells were electrode with the three electrode pattern and assembled into a test fixture as shown in Figure 2(a). The test fixture was used to test different drive and layout options for the three-electrode concept. A separate test fixture was also built to measure Plasma-shell drive charge for precise efficiency measurement. Figure 2(b) shows two green Plasma-shells operating at high brightness. The drive waveform was investigated to increase emission power and addressing speed.

During these experiments two plasma discharge operating modes were observed–a high-efficiency/high-brightness mode and a low-efficiency/low-brightness mode. A sustaining Plasma-shell can transition between these states under different drive conditions, and a series of experiments showed that the transition is affected by changes in drive voltage, drive frequency, and electrode geometry. It was concluded that high-efficiency mode can be stable at moderate drive voltage and frequency, and this operating point coincides with maximum emitted power. However, it was found that electrode

geometry must be carefully controlled to enable operation in the preferred mode. To this end, a novel three-electrode drive scheme was experimentally tested so that Plasma-shells operate in high-
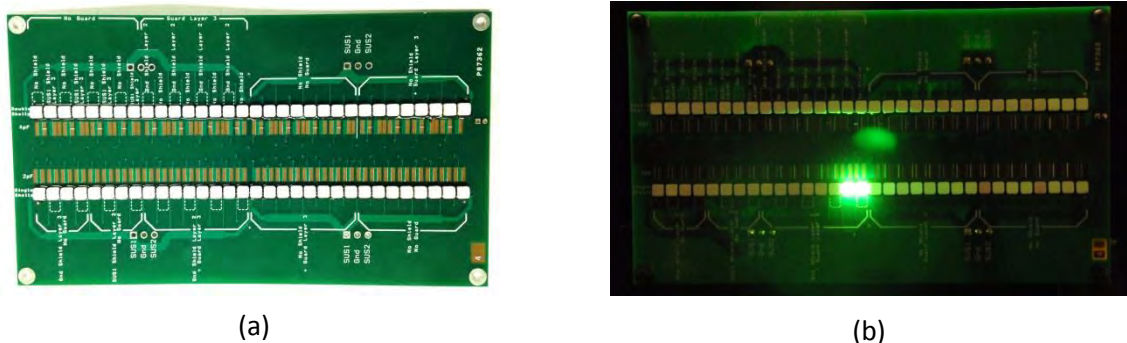




(a)

(b)

Figure 2. Fully populated three-electrode Plasma-shell test board: (a) off state; and (b) on-state emission of two addressed Plasma-shells with green phosphor.

brightness, high-efficiency mode with full addressability.

In an IR&D effort, the novel three-electrode drive scheme developed for this application was investigated for large-scale manufacturability. Figure 3 shows the prototype 2-inch cube that houses drive electronics and a three-electrode Plasma-shell array that emits UVA light at 350 nm wavelength. These shells were hand-painted with the required conductive and resistive inks. Drive electronics sustain shells with a 940 V square wave at 85 kHz, and shells operate in the high-efficiency discharge mode that produces 3.8 mW per shell. Refinement of the drive electronics and shell electrode geometry improved output power from a previous value of 2 mW per shell at 800 V, 120 kHz. While the UVA output power reported here is much higher than results achieved with UVC shells, improvements here will directly benefit UVC emitter arrays.



Figure 3. Prototype of a three-electrode panel and drive electronics that fits within a 2 inch cube.

Work was done on the step-up transformer used in the switching power supply, and by custom-winding bobbins for E-core ferrites with ratios between 22:1 and 30:1 were investigated. Higher voltage coupled into the Plasma-shells was demonstrated to improve output emission. However a significant improvement in UVC LED output, has led the team to conclude UVC LEDs are a better choice for use in the transceiver.

## Phosphors

DEI procured several UVC phosphors and tested them with vacuum UV (VUV) excitation. Available emission peaks include: 226 nm, 230 nm, 234 nm, 242 nm, and dual peaks of 253 and 273 nm. All phosphors had similar decay time constants of ~10 $\mu$s. Phosphor emission wavelengths and speed are suitable for medium data rate communication in wavelengths shorter than the best available UV LEDs.

3

## Life testing

The Plasma-shells have superior life, and may be of value in some applications. Aging data for UVC Plasma-shells manufactured at the start of Phase I are shown in Figure 4 where average power for two shells is normalized to burn-in time of 24 hours. Output power at 26,000 hours is 50% of initial power at 24 hours! This demonstrates that Plasma-shells have superior lifetime compared to UVC LEDs with lifetimes as short as 1000 hours.
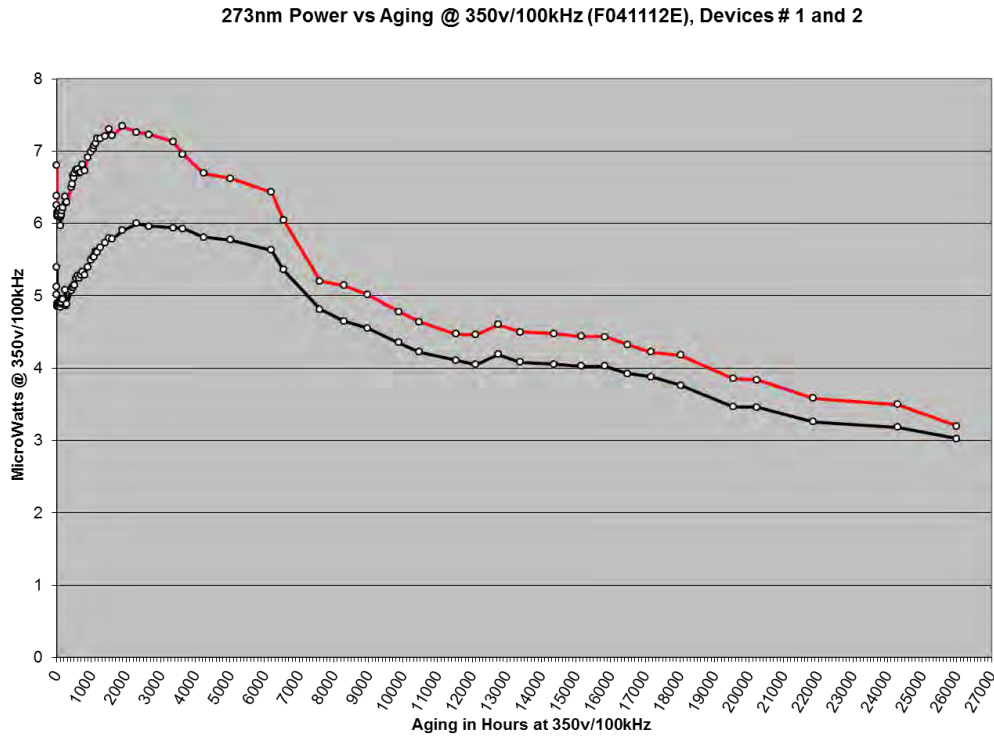
**273nm Power vs Aging @ 350v/100kHz (F041112E), Devices # 1 and 2**



Figure 4: Plasma-shell UVC power at 26,000 hours is greater than 50% of initial value.


## Task 3. Transceiver Hardware

The transceiver hardware was divided into four areas of investigation, the led, the photon counting device, solar blind filter, and the packaging. Progress on key components of the test bench is reported below:

## LED Driver Circuit

To improve LED drive waveforms, an improved pulsed driver circuit was designed and built to achieve faster turn-on/turn-off times by overdriving the LED during transitions. This allows higher modulation speed and more on time during each bit period enabling faster data links to accommodate communication overhead. LED optical emission needs to be observed during rising and falling edges in order to optimize the emission profile, so a silicon carbide (SiC) UV photodiode and amplifier module were constructed.

The communication test bench requires LED emitters that operate at the maximum thermal limit of the UVC LEDs, thus two new LED emitter modules were designed and built that include heat sinks with forced air cooling and integrated pulse driver circuits. The new driver circuit achieves drive current rise and fall time of 100 ns at peak current of up to 10 A.

4

The LED subassembly was miniaturized to the fullest extent using the Crystal IS LED with a customized heatsink and fan. Further optimizations have been identified and will be employed in future work.

A reduced-volume LED emitter shown in Figure 5 was designed and built around the new Crystal IS Optan UVC LED, which is their UVC LED die packaged in a hermetic TO-39 package with a ball lens that collimates output to 15° beam width. The custom heat sink and fan package provides optimal thermal management in a package of 25 cm on edge. It is believed that future fielded systems can achieve adequate LED thermal control without forced air cooling as LED efficiency improves, but the current fan is needed to operate with higher LED drive currents during developmental testing.



Figure 5: Reduced size LED emitter assembly with 5 mm LED, heat sink, and fan.

## Photon Counting Devices

DEI has been working with Hamamatsu and Photonis to investigate and acquire samples of planar photon counting devices such as the Hamamatsu micro-PMT, Photonis Planacon, and Photonis hybrid photodiode. We started with the Hamamatsu C9744 photon counting discriminator module that was reverse engineered so that a reduced-footprint circuit can be built into future hardware designs. The Hamamatsu unit also has a noise susceptibility problem that was corrected in DEI's design. Two photon discriminator circuits were designed in-house. The first design intended to duplicate the functionality of the Hamamatsu C9744 discriminator and eliminate its noise sensitivity problem. The second design was a bandwidth-limited trans-impedance amplifier whose output is digitized by a 12-bit analog-to-digital converter (ADC). DEI completed testing of an in-house photon discriminator circuit that achieves identical performance as the C9744 discriminator, and resolves the false-triggering problem. The design will be useful with multi-pixel photon counting sensors.

A major improvement of the transceiver architecture will be the use of the Photonis hybrid photodiode (HPD). The Photonis HPD was procured and support circuitry developed within the constraints of the budget. Hardware was designed and ordered for the Photonis HPD photon-counting sensor and initial testing begun. Long lead times for the Photonics HPD hindered the integration of this component into the breadboard transceiver module. Because the HPD sensor has 19 channels to digitize, a single-chip multi-channel discriminator IC would be an ideal solution to digitize the sensor output using a minimum of board space and power. Ultimately a custom ASIC will be required to realize the full potential of this device. This will be explored in future development efforts.

## UVC Filter

The PMT enclosure shown in Figure 6 was designed and built to protect the water-soluble UVC filter from humidity by sealing the PMT, UVC filter measuring 25 mm diameter × 15 mm thick, and desiccant pack in an air-tight compartment. The enclosure has mounting points for the PMT base, a laser sight for alignment, an iris to cover the filter, and a ¼"-20 threaded hole for tripod mounting. The assembly is completed utilizing the Schott UG5 black glass filter that blocks the visible passband of the UVC filter and is chemically stable for use as the outer window material. The UVC filter is a proprietary nickel sulfate ($NiSO_4$) material called UVC7 from INRAD Optics that is more stable across temperature and humidity exposure than pure nickel sulfate.

Spectral responses of three UVC filter stackups shown in in Figure 7 were measured with respect to the emission of a UVC Plasma-shell (e.g., the black reference line). Spectra provide limited information because they are near the noise floor of the spectrometer, and total light collection was affected by filter thickness, refractive index, and sidewall reflectivity. Despite this, it can be seen that the UVC7 filter passes the two UVC peaks and blocks everything except a wide passband around blue. The two black glass filters attempt to block the blue band and the UV11 material is far more effective than the UV5 material. It is likely that an organic filter material will be needed to provide additional attenuation at 300–350 nm. Further testing is needed to measure the combined response of the photon counting receiver module with filters.
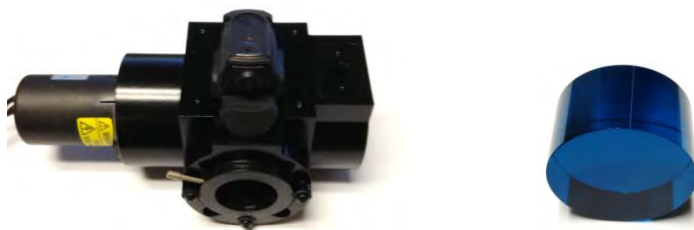


Figure 6. The custom air-tight PMT housing on the left protects the water-soluble UVC filter on the right.
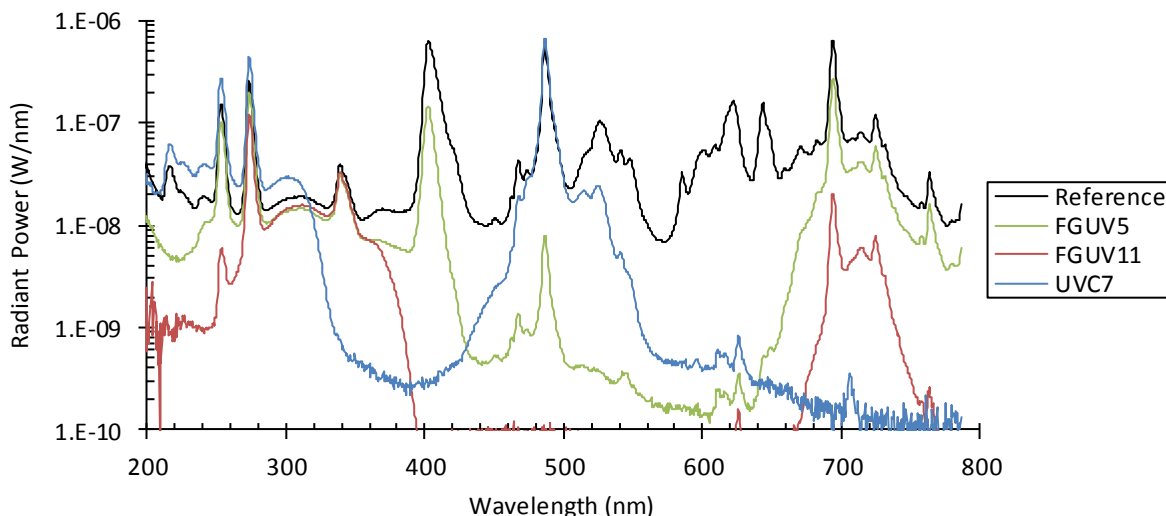


Figure 7. Spectra of UVC Plasma-shell light emission (e.g., reference line) through three filters: Schott UV5 (FGUV5), Schott UV11 (FGUV11), and INRAD UVC7. Multiple filters must be stacked to achieve an acceptable solar blind sensor response.

Two potential suppliers were identified: Ofil and Delta Imager. The solar blind filters available from Ofil are expensive at $17,000 per filter. Delta Imagers filters were $3,000 per filter. Subsequently DEI placed an order with Delta Imager for integration into the transceiver.

In parallel with this, DEI investigate SB filter prior art. Expired U.S Patent 4,317,751 and 4,597,629 issued to ITT provide a detailed description of a solar blind filter. In these patents, several filters are stacked to achieve the desired band pass. The chemical composition of each filter is defined. Additional research uncovered strategies for adjusting filter chemistries to further "sculpt" the pass band. The opportunity exists to develop a tailored filter optimized for a very narrow band of between 275 nm – 280 nm. This will be an important part of future optimization path.

## Packaging

The transceiver hardware was packaged to fit within a breadbox-sized volume of 12 in. × 6 in. × 6 in. The two UV transceivers were repackaged into a volume of 7.5" (L) × 5" (W) × 5.5" (H) as shown in Figure 8. This was achieved by integrating circuits and power supplies onto a reduced number of PCBs with cleaner interfaces. Key boards that were improved include the discriminator, the FPGA board, and the LED driver.
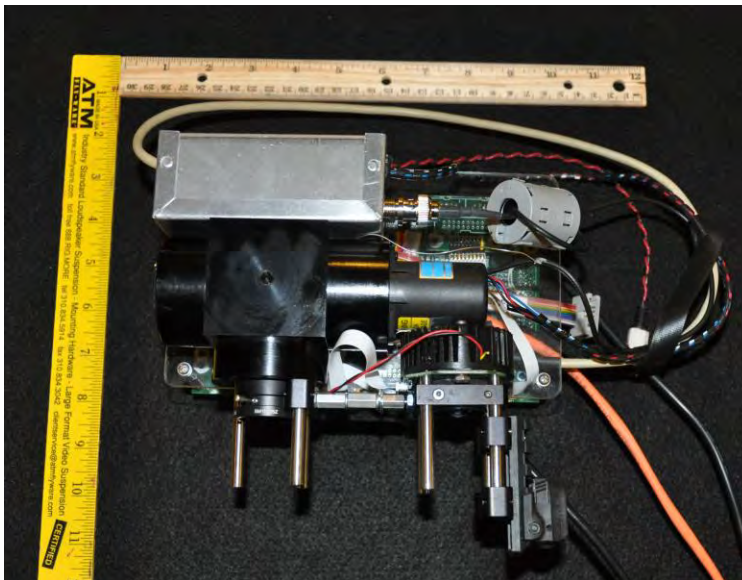


Figure 8: Reduced size transceiver hardware.

The discriminator was mounted in a shielded enclosure, and the discriminator circuit was integrated with its power supplies and the PMT power supplies on one board, and the output cable that goes to the FPGA logic was reduced to a single cable with signal and power. The FPGA board now includes the LCD interface board with mounting points (this is used as a convenient user interface during field testing), and it directly connects to discriminator board and LED driver board. The LED driver, which had been integrated with the LED and lens assembly, is now a separate board that mounts on the FPGA board and connects to the LED with a short cable to allow LED pointing. Minor bugs were addressed during the integration process. The repackaged modules still contain a significant amount of empty space and have the potential to be reduced in size much further in future development efforts. An Altera Cyclone V system-on-chip (SoC) was employed to further the integration effort. The SoC FPGA has a dense logic array and a powerful 32-bit processor in one package, and this will reduce part count for future single-board transceiver modules.

Two complete systems have been integrated into bread box sized enclosure with a small commercially available battery and charger to allow an untethered demonstration.  Figure 9 is a photograph of the transceiver system. In addition to the UV LED and the photomultiplier tube the system includes an LCD screen to display bioharness data, a tilt stand to position the system for test and evaluation and a strap handle for transportation. The system also includes a number of I/O ports for firmware updates, troubleshooting, and data collection.



Figure 9: Packaged UV NLOS transceiver.

## Task 4. Network Protocol

In this task, networking protocols were investigated to support the project objective of seamlessly integrating UVC communication nodes into complex multi-hop network architectures. The network protocol was simplified to a master-slave polling architecture to simplify implementation. Protocols were developed for packetization of data with an ACK/NAK response and automatic adjustment of signal levels until confirmation. Packets include routing information, payload, channel transmit and receive conditions and quality, and error detection. The packets allow for multiple-node communication. Bi-directional communication has been tested using a combination real channel (UV transmit and receive) and simulated additional channel using a cable, but with combined receive channels response to simulate the real conditions of half-duplex echo and collisions.

## Task 5. Testing

### Unidirectional Communication

Data flows in the clockwise direction, originating as a random number test vector on the left and being recovered and analyzed on the right. The test bench implements a basic data link operating at 50 kbps and measures noise counts (received photons and dark counts with the transmit LED off), combined

average signal and noise counts, and received BER. Calculated SNR and BER for many bits ($10^5$ in this test) are basic measures of link performance.

Measured SNR at three ranges is shown in Figure 10. The elevation angle of the transmit LED is indicated in the legend, as either pointed slightly over the receiver (10°) or aimed somewhat higher (30°). Average transmit power is doubled by using two LEDs, where each LED module transmits approximately 7 mW average optical power into the atmosphere. The PMT receiver is pointed at an elevation angle of 45° and is filtered by the UVC7 and black glass filters. The test was conducted at night because the current filter stackup is insufficient to fully reject daylight. With this test setup, BER was measured to be 0 for all points except those circled, where SNR was sufficiently low to experience errors. It can be seen that the system requires a SNR of at least ~9 dB to operate, and this can be reduced to closer to 1–2 dB using improved coding. This would enable a significant reduction in transmitted power.
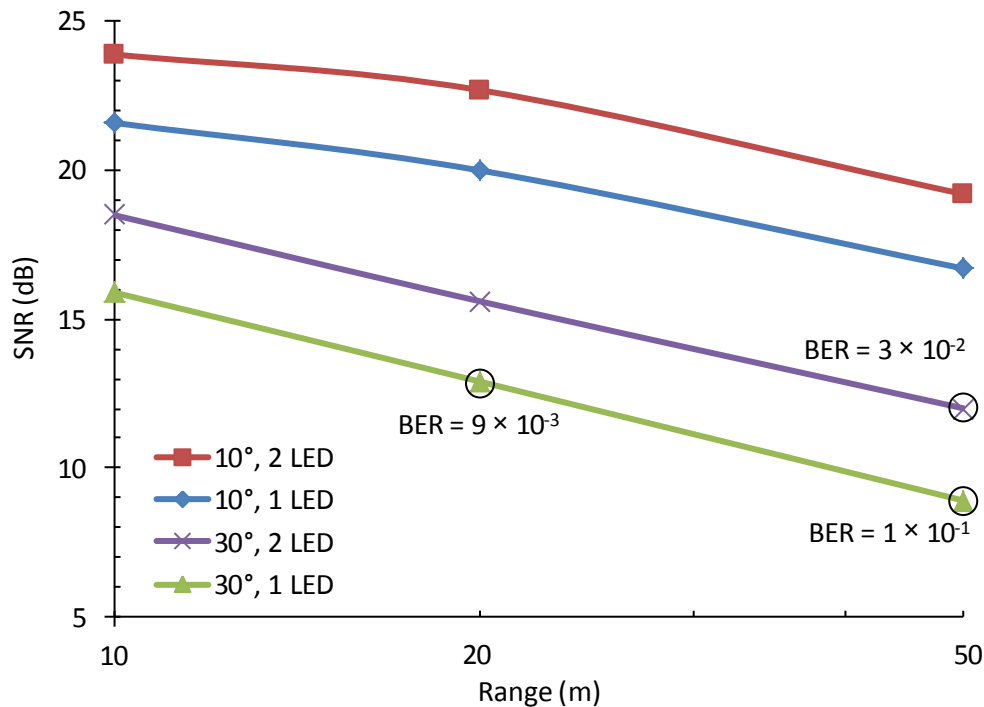
Figure 10. Test data showing SNR versus range with BER.

The test bench software was updated to implement AES-128 encryption on payload packets. The AES cipher is NSA approved for classified information: 128-bit key length is sufficient for SECRET level, and 192- and 256-bit key lengths can be used for TOP SECRET information.

After testing was completed, the hardware test bench was tested with two additional functions: real-time data transfer of medical data, and encryption. The test bench diagram in Figure 11 shows the hardware and software configuration several months after testing. Real-time patient vital sign data is imported from a Zephyr Bioharness into MATLAB where patient data is packetized and encrypted. Packets are framed and modulated prior to transmission by the FPGA board. The reverse process is applied at the receiver and the real-time medical data stream is presented on a dashboard graphical interface.
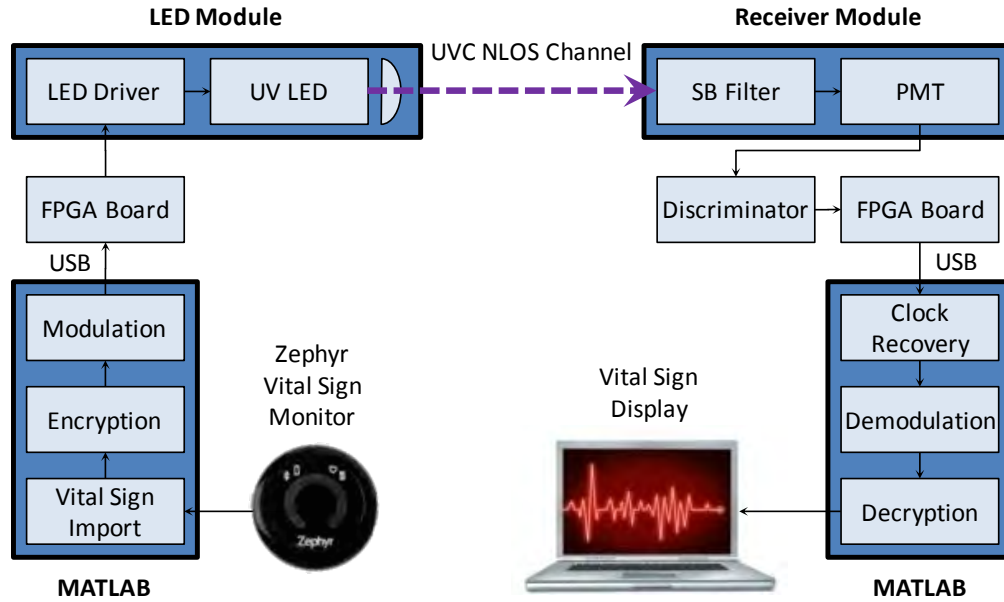
Figure 11. Test bench configuration for real-time transfer of secure (encrypted) medical data from a Zephyr Bioharness for display on a remote laptop.

## Network Protocol Testing

A Benedict computer model DLM400 serial protocol analyzer was purchased for testing Bit-Error-Rate (BER) between the units. A BER test packet was sent repeatedly by the DLM400 to one unit, via RS422, transmitted to the other unit, then back to the DLM400 over RS422 for analysis. The baud rate was 57600. The results are summarized in Table I below. The general results are that no errors occurred. This is due to the built-in cyclic redundancy check (CRC) in the UVNLOS protocol. It will not knowingly emit a corrupted packet through the RS422 port. Data will not be sent unless the entire packet including CRC is correct. The corrupt packet will be ignored, and then re-transmitted by the sender at increased UVC power level. As the packet error rate increases, the endpoint throughput decreases due to the increased number of re-transmitted packets. The addition of forward error correction to the protocol will allow the units to transmit at the minimum power level to achieve the required data throughput.

Table I. Results of Bit Error Rate Test

| | |
|---|---|
| Chars sent | 51200 |
| Char Recv | 51200 |
| Rec in sync | 51200 |
| Elap Second | 23 |
| BERT (%) | 0 |
| Average trip time per block (ms) | 237 |
| Block Error | 0 |
| Bit errors | 0 |
| Blocksize | 512 |
| Error Free Sec (%) | 100 |
| BLERT (%) | 100 |

10

## UVC Effect on Night Vision Goggles

A basic test was done to estimate the effects of UVC emissions on night vision goggles (NVG). Helicopter pilots use the AN/AVS-6 aviator's night vision (ANVIS) goggles that use third generation (Gen 3) image intensifier tubes to greatly amplify ambient light. A unique feature of AN/AVS-6 goggles is the incorporation of a "blue-cut" filter on the objective lens that blocks nearly all light of wavelengths shorter than 625 nm. The purpose of this filter is to allow internal aircraft lighting and displays to be viewed by the naked eye using shorter wavelength colors such as green, yellow, and blue, while outside scenery is viewed through NVGs that amplify red and near infra-red wavelengths that are the dominant illumination wavelengths from moonlight and starlight.

The test setup in Figure 12 was used to measure visual acuity in low-light conditions. It is intended to estimate the effect of a UVC transmitter illuminating the cockpit and windshield from a distance of 1 meter, potentially interfering with observation of the instrument cluster and outdoor scene. A Snellen-style eye chart was scaled for use at 1 m and printed on a white sheet, and the chart is illuminated by a red LED that represents the outdoor scene with low ambient light levels. For reference, starlight radiance is 0.002 Cd/m$^2$ and moonlight can be as bright as 1 Cd/m$^2$. Eye chart radiance was spot-checked with a hand-held light meter. The eye chart was additionally illuminated with a UVC LED, and a bandpass filter was included to limit emission wavelengths to 270 ± 10 nm. The minimum required LED transmit power for indoor environments is estimated to be 50 µW for 50 kbps communication over 1 m, and this test was conducted at a level 1600× greater than this power level in order to have an observable effect. Direct UVC illumination on the chart was equivalent to a powerful 84 mW source with a 30° beam angle. The visual acuity of a human observer was measured at 1 m distance using the standard Snellen pass criteria of 5 out of 6 correctly identified letters per row.
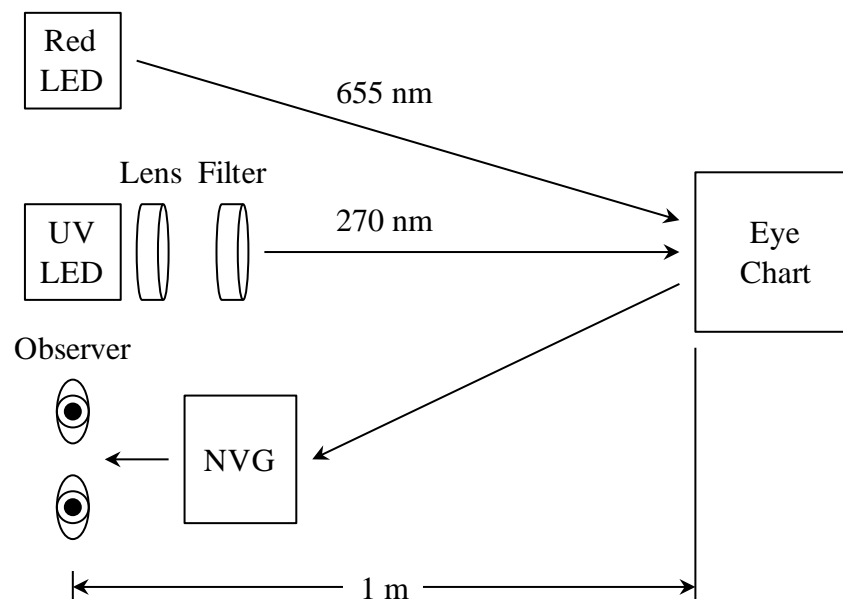


Figure 12: NVG compatibility test setup.

Visual acuity was measured at different ambient light levels, with and without UVC illumination. The visual acuity of the observer was 20/20 with normal white lighting and chart radiance of 44 Cd/m$^2$. Table II shows that strong UVC illumination had no effect on visual acuity, and was barely discernable

11

even at the lowest tested light level that is below starlight illuminance. In fact, even with the red LED turned off and only stray light illuminating the chart, acuity was measured at 20/200 and added UVC illumination did not improve acuity.

Table II. Visual acuity versus ambient light level.

| UVC Light | Red Light Intensity: | | |
|:---:|:---:|:---:|:---:|
| | 0.1 Cd/m$^2$ | 0.01 Cd/m$^2$ | 0.001 Cd/m$^2$ |
| Off | 20/40 | 20/30 | 20/50 |
| On | 20/30[1] | 20/30[1] | 20/50[2] |

Note 1: Could not see UVC light at all.

Note 2: UVC light was barely perceptible; no effect on letter recognition.

Our conclusion from this experiment is that an active UVC emitter, even when emitting far above the minimum required power level and directly illuminating visible surfaces, does not affect visual acuity in low light environments. It is not expected to interfere with visual tasks and did not cause NVG blooming or blinding. It appears from this testing that the NVG has excellent UVC rejection.

## Brassboard Demonstration

A brass board implementation was realized that included packaging of the tranciever and battery into a breadbox size system. The systems were integrated with a Zephyr bioharness and biometric data was successfully transmitted at a rate pf 57K BAUD. The Zephyr bioharness protocol was analyzed and linked using its standard Bluetooth communication interface to one of the units, displaying the relevant data and simultaneously transmitting to the other unit over the UVC link.  Both units then display the bioharness data. Figure 13 is a screen shot of the bioharness data display that has been and received via a NLOS UV unit.
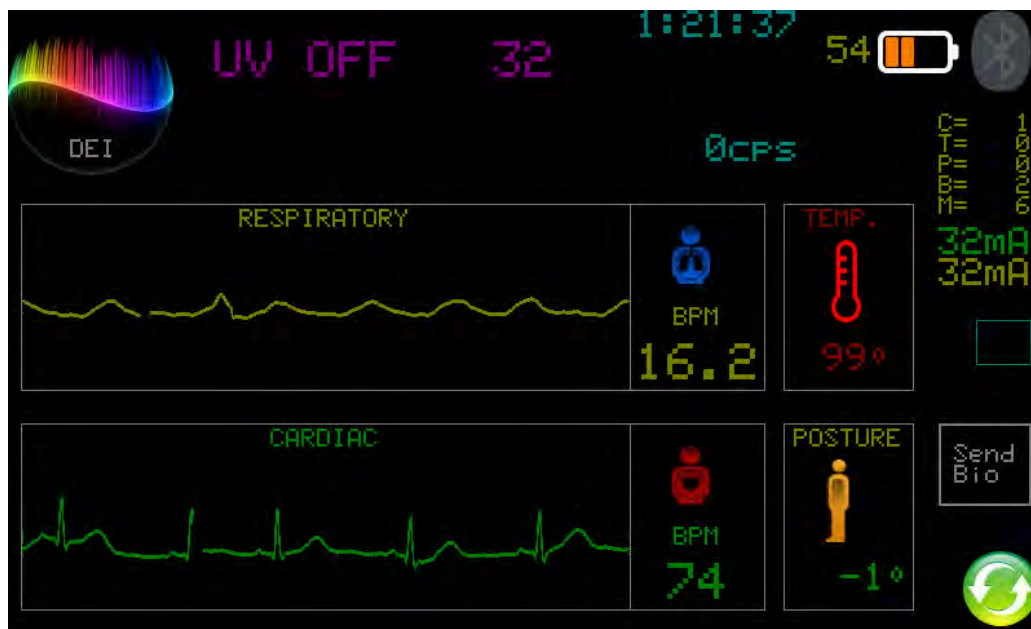


Figure 13: Bioharness data transmitted and displayed via UVNLOS transceivers.

The software and FPGA equations was "cleaned-up" to make room for the demonstration software. Old test-performing code and display features were removed and replaced with a new GUI-like control panel emphasizing the bioharness link feature.

### Prototype demonstrated

Two breadbox sized communication systems (Figure 9) were integrated and demonstrated non-line-of-sight bidirectional communication at Ft. Detrick. One of the transceivers was connected to a Zephyr bioharness worn by IST personnel. Biometric data was transmitted in real time from one system to the other.

# Key Research Accomplishments

- Successfully demonstrated unidirectional and bidirectional communication at medium data rate communication link.
- UVC-emitting Plasma-shell
  - Demonstrated lifetime exceeding 26,000 hours (and counting).
  - Manufactured 3-electrode Plasma-shell array packaged within a 2-inch cube enclosure
  - A pathway to short-wavelength (< 240 nm), high-efficiency (> 25%) Plasma-shell emitters was identified.
- Established relationships with key suppliers and interested parties
  - Microtech, for high-volume electroding of Plasma-shells
  - UVC component manufacturers: Photonis, Hamamatsu, Crystal IS
  - Potential applications: Robotics Research LLC, Think-a-Move Ltd., and Engility Corp.
- Proposed networking protocols compatible with existing networking technologies
  - MATLAB GUI was implemented to allow on-the-fly communication configuration of: selectable number of packets; modulation type; LED duty cycle and LED current; vital sign statistics; and link statistics such as BER, signal strength, and photon counts.
- Integrated two portable NLOS transceivers in breadbox sized system capable of bidirectional communication at 57K BAUD
- Interfaced NOLS transceivers to Zypher bioharness and transmitted relevant real-time biometric data
- Identified clear path toward reduced size and weight of transceiver

# Reportable Outcomes

- The state of Kentucky awarded $500,000 of matching funds under Grant Agreement KSTC-184-512-13-167 to develop and commercialize this technology. As a result, the Phase II contract was novated to the newly created Kentucky-based subsidiary company DEI that was formed to develop and commercialize this technology.
- DEI hired Dr. Almalkawi as full-time researcher for this project. His background in communication systems will benefit all aspects of this project.
- DEI attended the SOCOM Tactical Assault Light Operator (TALOS) industry collaboration event at MacDill AFB November 19-20, 2013. UVC NLOS communication was proposed as a method for covert data communication integrated into a battle suit. There was interest in NLOS technology for security products and UAV command and control.

- DEI attended the C4ISR medical exercises on July 23, 2014 at Fort Dix. Observations of medical exercises and interviews of program officers and enlisted personnel have been beneficial for understanding intended use cases for this technology.
- Submitted 2nd Phase II SBIR for UVNOLS and was subsequently given notice of award
- Recent commercialization activities of synergistic UV Plasma-shell technology:
  - Contracted by Aquionics to produce UVA Plasma-shell modules for UV sterilization.
  - Contracted by EPA to produce UV Plasma-shell water purification modules.

## Summary and Conclusion

The UV spectrum is currently unused and is not susceptible to RF interference, jamming, or microwave attack. This presents opportunities for achieving covert communication especially in situations requiring radio silence. Potential applications beyond combat casualty care include: voice communication within fire teams and squads; unmanned aerial/ground vehicle (UAV and UGV) operation; convoy networking, and unmanned ground sensor (UGS) networks. During this investigation, the required networking theory, prototype hardware and firmware of UV NLOS optical communication system was investigated, and a hardware and software brassboard was successfully implemented. A strategy to reduce weight and size of the brassboard was identified and will be implemented in the second Phase II.

## List Of Personnel Who Have Worked On The Effort
- Guy, J.
- Cross, L.
- Peters, E.
- Alkhateeb, N.
- Afzal, R.
- Almalkawi, M.
- Wenzlaff, R.
- Cross, P.
- Butcher, J.
- Butcher, A.
- Wedding, C.
- Kurtz, A.